

EXPERIMENTAL INVESTIGATIONS OF AN ELASTO-FLEXIBLE MORPHING WING CONCEPT

B. Béguin, Ch. Breitsamter, N. Adams
*Institute of Aerodynamics, Technische Universität München,
 Boltzmannstr. 15, 85747 Garching, Germany*

Keywords: *Morphing wing, membrane wing, flow control, aerodynamic efficiency*

Abstract

This paper discusses the design and testing of an elasto-flexible morphing wing configuration allowing massive variation of the wing planform. The wing structure consists mainly of an articulated leading edge spar over which an elastic skin is spanned, forming the actual aerodynamic surface. The configuration of the leading edge spar, actively controlled, sets the overall planform of the wing whereas the elastic membrane just passively deforms under aerodynamic loading.

A wind tunnel half model of the wing was tested at three different wind speeds. Results from force measurements show the dynamic pressure dependency of the aerodynamic characteristics due to the high flexible wing construction. Also, the comparison of the drag polars of three different configurations of the wing show that planform morphing effectively provides significant variation in lift and drag characteristics, thus allowing to improve aerodynamic efficiency over a variety of missions.

1 Introduction

1.1 About morphing

The aerodynamic performance of an aircraft is strongly related to its geometrical configuration. The final layout of a given airplane is the result of an extensive design process, generally leading to a very efficient vehicle at the nominal operation point. However, performances may drop drastically at off-design conditions.

A modern trend in aircraft design aims at developing so called "morphing airplanes". Basically, morphing means being able to reconfigure the airframe geometry to improve performances over a variety of flight conditions, thus expanding the flight envelope. Such vehicles are obviously of great interest, since they could accomplish efficiently a variety of mission roles during a single flight for which a complete fleet of specifically designed airplanes would be normally required. Designing morphing aircraft raises new challenges for which the classical design methods and available technologies are not enough advanced yet. New structures, materials, control and actuation systems have to be developed in order to make morphing airplanes successful. In recent years, several universities, companies and government agencies have been spending an increasing amount of resources on morphing technology. An overview of the state-of-the-art in morphing research is given in [3] and [6].

In this context, the present paper concentrates on the design and testing of an elasto-flexible morphing wing concept taking advantage of sailing wing structures.

1.1.1 Aerodynamic efficiency

The essence of performance improvement through morphing can be assessed looking at the equation of the drag polar (Eq. 1). This basic relation describes the lift and drag characteristics of a given airplane and therefore directly influences the performance such as endurance and

range [1].

$$C_D = C_{D0} + KC_L^2 \quad (1)$$

The geometry sensitivity of the drag polar is expressed by the parameters C_{D0} and K since they are direct functions of the vehicle configuration. Roughly, the drag coefficient at zero lift, C_{D0} , contains the friction and parasite drag and therefore depends on the airplane's wetted and sectional area. The drag-due-to-lift factor, K , depends more generally on the aspect ratio (AR) of the vehicle.

The ability of morphing vehicles to transform their shape allows to adapt the lift and drag characteristics to a variety of mission requirements.

1.1.2 Maneuverability

Aerodynamic efficiency is obviously not the only design requirement of an airplane. Since stability derivatives are also strongly coupled with the airframe geometry, morphing also allows the airplane to reach different maneuverability levels, depending on missions requirements. Typically, configurations of high aerodynamic efficiency (high aspect ratio, large wing span) exhibit limited maneuverability because the associated high inertia and structural loading occurring while carrying out rapid maneuvers restricts the agility. In contrast, high agility configurations are typically associated with low aspect ratio and therefore show decreased aerodynamic efficiency. Since the geometrical features providing high efficiency limit high maneuverability and vice versa, targeted morphing can allow a single airplane to fly drastically different missions within a single flight.

1.2 About sailwings

Sailwings are elasto-flexible wing structures. They consist basically of a leading edge spar and trailing edge wire around which a membrane is spanned to form the actual aerodynamic surface, Fig. 1. The aerodynamics of sailwings is dominated by aero-elastic effects and therefore differs passably from conventional rigid wings.

The most influencing design parameters of a

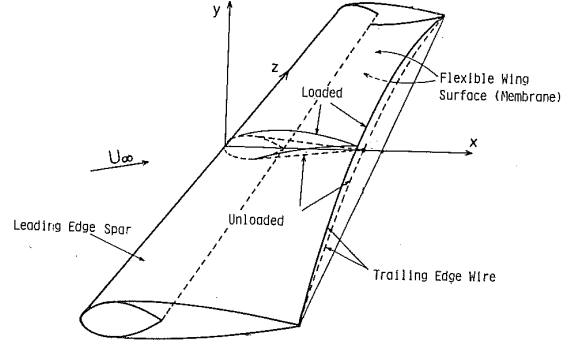


Fig. 1 Schematic figure of a sailwing structure [4]

sailwing are the geometry of the leading edge spar on the one hand, and the elasticity of the membrane on the other hand. The cross section of the leading edge spar is known to have a significant influence on the pressure distribution over the wing [4]. In fact, the discontinuity in curvature at the point where the membrane separates from the leading edge spar induces a sharp adverse pressure gradient favoring flow separation. An adequate geometry (i.e. asymmetric) can help reducing these discontinuities to obtain superior aerodynamic characteristics.

Beside this, the elasticity of the membrane plays an important role in sailwing aerodynamics since its interaction with the air flow influences the amount of deformation of the loaded membrane. Mainly, the deformation leads to non-linear lift characteristics as well as mitigated stall behavior. The latter is known as the passive flow control mechanism of sailwings [7], [8].

In order to assess the relative importance of aerodynamic over elastic forces in the membrane of a sailwing, the dimensionless membrane elastic constant \tilde{K}_m is introduced here:

$$\tilde{K}_m = \frac{K_m}{q_\infty \cdot \bar{c}} \quad (2)$$

where q_∞ (N/m^2) is the free stream dynamic pressure, \bar{c} (m) is the mean aerodynamic chord of the wing and K_m (N/m) the elastic constant of the membrane. This "fictive" membrane constant gives an assessment of the amount of deformation to be expected or, in other words, how far the behavior of the wing will differ from the one

of an equivalent rigid wing (i.e. $\tilde{K}_m \rightarrow \infty$). The lower the value of \tilde{K} (i.e. high dynamic pressure or very elastic membrane), the higher the aero-elastic effects influence the wing behavior.

1.3 The elasto-flexible morphing wing

1.3.1 Description of the concept

The biologically inspired morphing wing concept dealt with in this paper takes advantage of sailwing structures to simulate roughly the skeletal/skin structure of a pterosaur [5]. A sketch of the concept is given in Fig. 2. The main structure consists of an articulated leading edge spar, over which an elasto-flexible membrane is spanned forming the actual aerodynamic surface. An application field for this wing is typically low-speed unmanned air vehicles (UAV's).

The configuration of the leading edge spar,

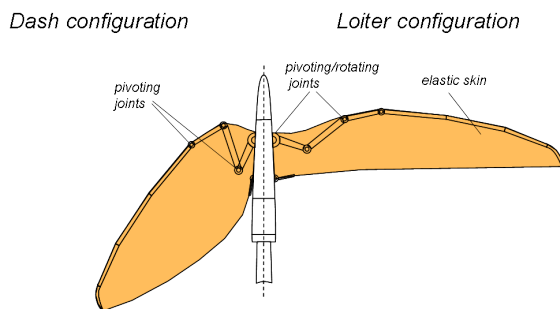


Fig. 2 Sketch of the morphing concept

consisting of four segments connected to each other by pivoting joints, sets the overall geometry of the wing. These segments can be compared respectively to the upper arm, lower arm, hand and finger of the biological paragon. Additional rotating joints are included at two locations (shoulder and finger) of the leading edge spar to allow to twist the wing for control or trim purpose. Finally, this design allows the wing to undergo up to 100% change in aspect ratio as well as 40° variation in sweep.

On the one hand, the use of an elastic membrane for the wing surface is chosen to obtain an aerodynamic surface able to adapt to the massive form variation. On the other hand, the membrane spanned over the structure provide a seamless

aerodynamic surface while undergoing shape change. As mentioned earlier, the aerodynamic behavior of sailwings may differ passably from the one of rigid wings. However, in this concept, the non-conventional behavior of sailwings should offer advantages to provide the wing with additional morphing capabilities. The passive morphing of the membrane is known to feature interesting stall characteristics. Regarding a further concept stage, the integration of actuators in the membrane could allow for active morphing of the wing surface.

1.3.2 Wind tunnel model

A wind tunnel half model with a maximum span of 1 meter was designed and built for the experimental investigation of this concept. The leading edge spar features an asymmetric cross-section in order to reduce sharp suction peaks that are likely to occur by sailwings with rounded or symmetrical cross section.

Linkages introduced between the segments of the leading edge spar coordinate their relative movements in such a way that the configuration of the whole structure is predetermined by the angular position of the shoulder joint, actuated through an embedded stepper motor. The trailing edge consists of a telescopic bar which length adapts to the current configuration. Finally, the whole structure is fixed to a bed plate allowing to mount the model in the wind tunnel test section. Fig. 3 shows the frame structure of the model in three configurations.

For the membrane, a suitable elastic and impervious fabric found in commerce is used. It consists of a stretchable woven fabric, coated on one side with a polyurethane (PUR) layer [2]. The wing surface then consists of a sewed pocket of this material, imposed over the structure and spanned at the wing root. The specifically designed cut of the membrane avoid the formation of wrinkles and ensure a certain pretension level at all configurations. At this stage of the project, the membrane does not involve any stiffening elements or actuators for active camber morphing

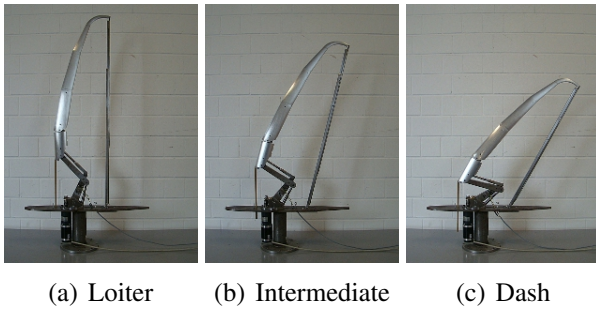


Fig. 3 Frame structure of the model

but is just a passive element.

Finally, the morphing capabilities of this model

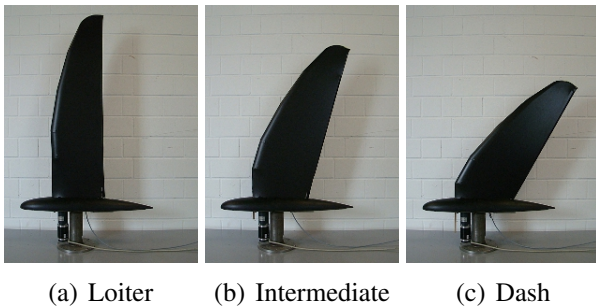


Fig. 4 Complete model with membrane in three configurations. A generic fuselage covers the shoulder joint and wing root plate

in terms of the allowable variation in aspect ratio AR , sweep angle $\phi_{1/2}$, wing area S and span b are given in Fig. 5. The achievable configurations vary continuously between a high aspect ratio ($AR = 8.56$), straight wing ($\phi_{1/2} = 6^\circ$) and a low aspect ratio ($AR = 4.59$) swept-back ($\phi_{1/2} = 36^\circ$) configuration¹.

2 Wind tunnel testing

2.1 Test setup

The morphing model presented above is tested in the subsonic wind tunnel facility "A" (opened

¹This achievable range of configurations is conditioned by the linkages between the segments of the leading-edge spar. Planforms out of the range presented here could be obtained by moving each joint independently.

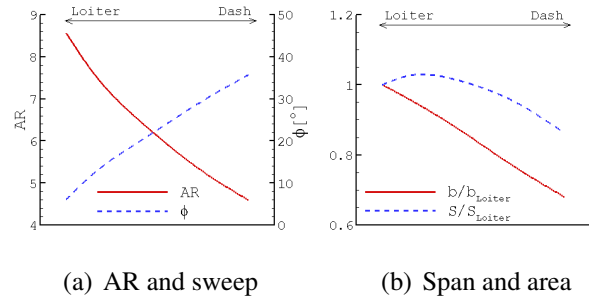


Fig. 5 Morphing capabilities of the wind tunnel model

test section) of the Institute of Aerodynamics of the Technische Universität München. The size of the test section is 1.8 m x 2.40 m, and the maximum wind speed is around 65 m/s corresponding to dynamic pressure up to 2500 Pa. Fig. 6 gives a view of the model mounted on the underfloor (external) balance in the wind tunnel test section.

A total of five discrete configurations are ex-



Fig. 6 Morphing model in the wind tunnel (intermediate configuration)

perimentally investigated including both extreme configurations (loiter and dash) and three in-between configurations. Tests are performed at three different wind speeds, namely 15, 22.5 and 30 m/s corresponding to mean aerodynamic chord (\bar{c}) based Reynolds numbers of 230000, 345000 and 460000, respectively. Although this Reynolds number range is relatively low, transition strips are not used. Tests with a microphone probe at 0° , 5° and 10° angle of attack show

that transition occurs within 25% of the chord at all wind speeds for the swept back configuration whereas the boundary layer may stay laminar over up to 75% for the loiter configuration. Force measurements are performed in order to assess the overall aerodynamic behavior of each configuration as well as the features provided by planform morphing. For this, the model is fixed in the wind tunnel to a 6-component aerodynamic external balance. In order to avoid interactions of the model with the boundary layer developing on the floor of the test section, the model is elevated by around 14 cm from the floor and a so called "péniche" covers the portion of the fixation shaft exposed to the airflow (see Fig. 6). Thereby, the péniche is fixed to the floor of the wind tunnel but is not in contact with the model. Polars from -20° to $+40^\circ$ angle of attack (α) are measured. This relatively wide range of angles of attack is chosen in order to capture the complete stall behavior of the wing, since sailwings should provide noticeable stall characteristics. At each angle of attack, averaged forces over 30 seconds are recorded. Finally, Table 1 gives a summary of the tested cases.

Investigation of the flow pattern at the surface of

$U_\infty [m/s]$	Re	$q_\infty [Pa]$	\tilde{K}_m	α range
15	230000	145	20	-20° to $+40^\circ$
22.5	345000	310	10	-20° to $+40^\circ$
30	460000	545	5.5	-20° to $+40^\circ$

Table 1 Test matrix

the wing is also performed using the wool tufts method. For this, wool threads are stitched into the membrane and photographs of the wing at different flow conditions allow to visualize the areas of separated flow (see Fig. 7).

Finally, pictures of the wing are taken with a camera showing in span-wise direction and fixed above the wind tunnel to assess the deformation of the wing surface at different flow conditions. Only the loiter configuration is investigated with this method, since its straight wing geometry facilitates the assessment of the deformation. Moreover, the phenomena observed on the loiter configuration are supposed to apply at least qual-

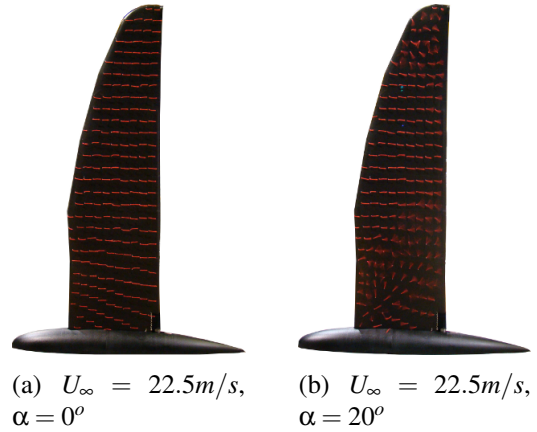


Fig. 7 Suction side of the model with the threads stitched in the membrane

itatively to the other configurations as well.

3 Measurement Results

Here, the measurement results are presented for the loiter, dash and an intermediate configuration. Table 2 gives a summary of the geometrical parameters of these three configurations.

Configuration	AR	$\phi_{1/2}$	b/b_{loiter}	S/S_{loiter}
Loiter	8.56	6	1	1
Intermediate	6.38	20	0.87	1.01
Dash	4.59	36	0.68	0.86

Table 2 Geometrical parameters of the three wing configurations selected to present the measurement results

3.1 General behavior of the elasto-flexible wing

3.1.1 Assessment of wing deformation

Fig. 8 shows the loaded shape of the suction side of the wing (loiter configuration) at 10° angle of attack for the three investigated wind speeds. Clearly, increasing the dynamic pressure (i.e. reducing the fictive membrane constant \tilde{K}_m) significantly affects the shape of the wing. Sequential processing of these pictures for angles of attack from 0° to 40° allowed to follow the evolution of the amplitude of the camber as the angle of attack changes. The result is given in Fig. 9. This

graph will be commented on later in more detail in relation to the force measurements. Although only the deformation of the loiter configuration is presented here, the same trends are supposed to apply for the other configurations.

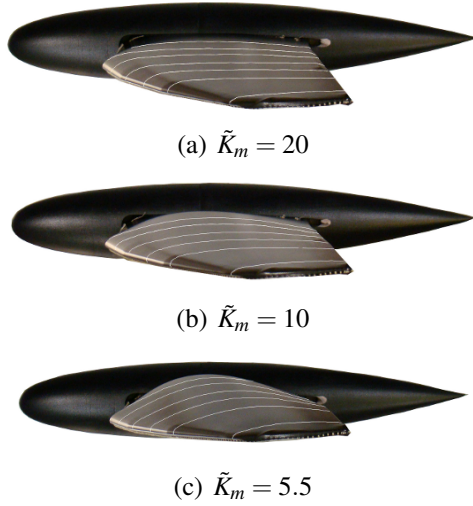


Fig. 8 Visualization of the deflected suction side of the loiter configuration for different aerodynamic loading ($\alpha = 10^\circ$).

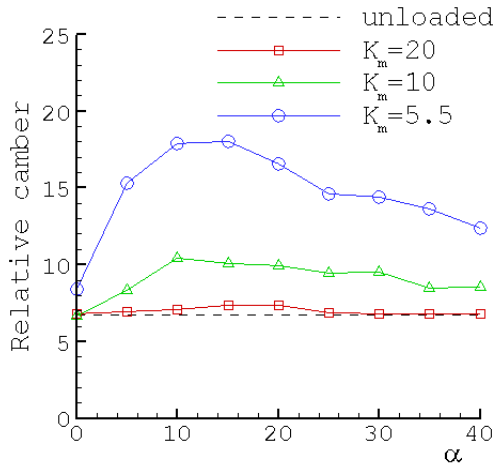


Fig. 9 Evolution of the maximal relative camber of the suction side (in percent of the mean aerodynamic chord)

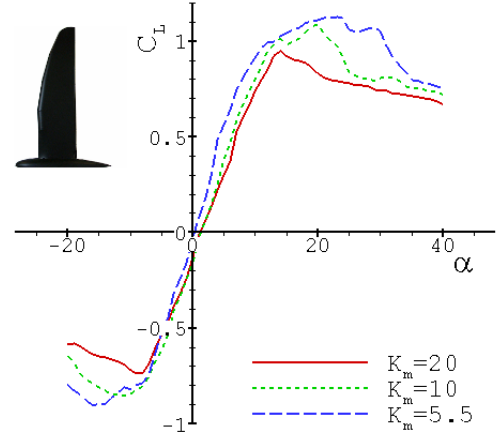


Fig. 10 Lift curve (loiter configuration)

3.1.2 Lift characteristics

Fig. 10 shows the measured lift curves of the loiter configuration². The $\tilde{K}_m = 20$ lift curve is largely linear before the onset of stall since the wing does not deform significantly in this case (see Fig. 9). Thus, the wing behaves more like a rigid one at this relatively high value of \tilde{K}_m .

As the dynamic pressure is increased, the lift

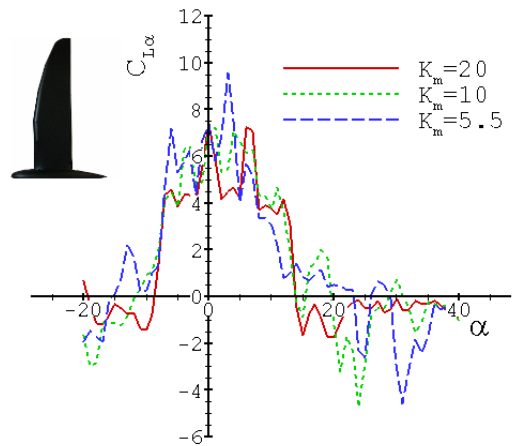


Fig. 11 Slope of the lift curve (loiter configuration)

curve becomes non-linear as a result of the significant angle of attack dependent deflection of the membrane (Fig. 9). The slope of the lift curve

²The slightly negative zero-lift is due to asymmetries in the flexible model. Also, repeated measurements indicated a maximal discrepancy in lift of $\Delta C_L = \pm 0.04$ and in drag of $\Delta C_D = \pm 0.005$.

($C_{L\alpha}$, Fig. 11) is then closely related to the evolution of the camber: from 0° to about 10° , the camber grows and the lift curve exhibits a steeper slope than the $\tilde{K}_m = 20$ case. From about 10° and higher, due to the onset of stall reducing the aerodynamic load in the membrane, the camber decreases, leading to a lower $C_{L\alpha}$.

This natural camber adaptation to the current flow condition allows the wing to sustain a certain amount of lift even after the onset of stall and leads to noticeable stall characteristics. In fact, the stall occurs surprisingly late and rather smoothly for a straight wing at this low Reynolds number. However, this passive flow control mechanism becomes significant only after a certain amount of deformation. Here, this behavior is therefore especially pronounced in the case $\tilde{K}_m = 5.5$: compared to the $\tilde{K}_m = 20$ curve, the $\tilde{K}_m = 5.5$ one shows a delayed stall of about 10° and an increase in C_{Lmax} of about 0.2.

Fig. 12 shows the separation lines of the loiter configuration obtained from the wool tufts experiment. In the 15 m/s case, the separation begins at $\alpha = 10^\circ$ at the root of the wing as expected for a straight wing. Another separation spot appears at the tip of the wing at $\alpha = 15^\circ$ (maximum lift). After this, both regions of separated flow grow to finally lead to the stage of completely separated flow at $\alpha = 25^\circ$.

The separation process looks quite different for the 30 m/s case. The separation begins earlier ($\alpha = 5^\circ$) in the inner part of the trailing edge, certainly caused by strong adverse pressure gradients that are likely to occur in this part of the wing as a result of the high camber (see Fig. 9). As α increases, the separated flow region reaches the wing root and travels toward the leading edge (no separation spot at the wing tip in this case). However, this occurs very slowly compared to the 15 m/s case owing to the passive morphing of the membrane. For angles of attack above $\alpha = 15^\circ$, the decreasing camber may attenuate the adverse pressure gradients at the rear part of the wing thus retarding the propagation of the separation toward the leading edge. In fact, the flow is completely separated only for angles of attack above $\alpha = 30^\circ$.

The intermediate and dash configurations show

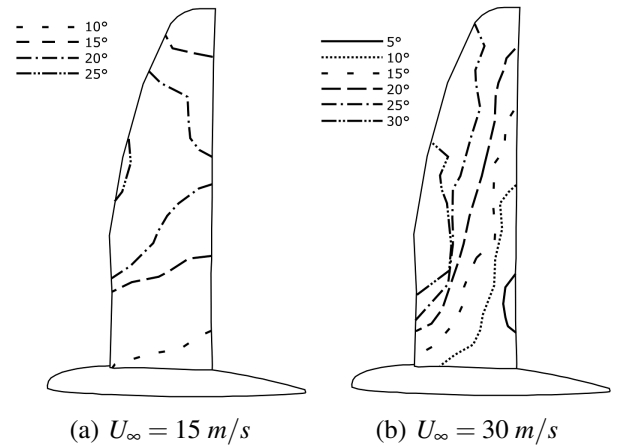


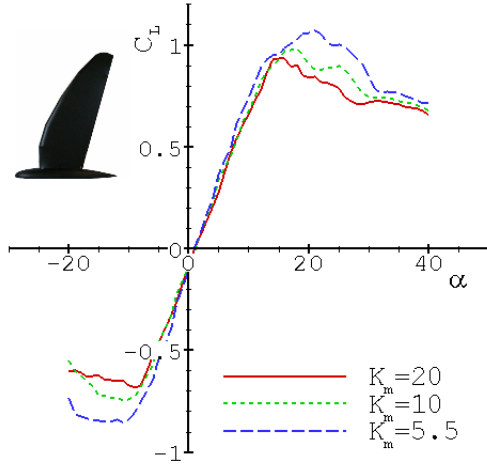
Fig. 12 Separation lines on the suction side of the loiter configuration.

similar behavior and are therefore not presented in detail here. Their respective lift curves are given in Fig. 13 a and b.

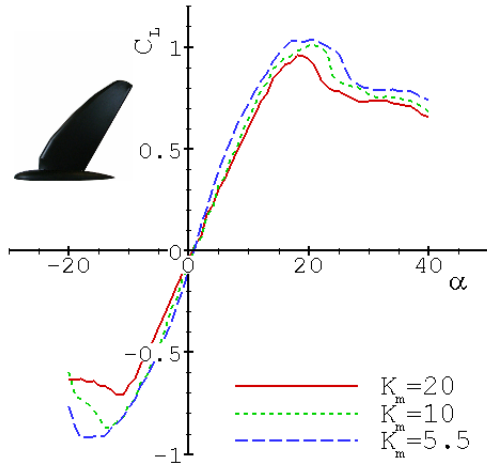
3.1.3 Drag polar

Fig. 14 shows the drag polars of the loiter configuration for the three investigated wind speeds. The influence of the membrane deformation is also clearly visible here and, interestingly, the wing features a lower drag at higher dynamic pressure. Beside a certain Reynolds number effect, this is attributed to the passive morphing of the membrane: as the aerodynamic loading increases, the resulting wing shape may lead to more efficient airfoil characteristics than the unloaded one. In fact, the plots of the lift-to-drag ratio (L/D) in Fig. 15 show that the loiter configuration at $\tilde{K}_m = 20$ (lowest aerodynamic load) features a lower efficiency over the whole angle of attack range.

For the intermediate and dash configurations, the same tendencies regarding the drag polars are observed. Fig. 16 shows the variation in $(L/D)_{max}$ with the dynamic pressure for the three configurations. The loiter configuration reaches the maximum ($(L/D)_{max} = 19$) at $\tilde{K}_m = 10$, meaning that the resulting wing shape at this aerodynamic loading may be optimal regarding the efficiency. For both the intermediate and dash configurations, $(L/D)_{max}$ monotonically increases with de-



(a) Intermediate configuration



(b) Dash configuration

Fig. 13 Lift curves of the intermediate and dash configurations

creasing \tilde{K}_m so that the maximum may be reached at a dynamic pressure out of the investigated range. However, both configurations feature a maximum $(L/D)_{max}$ around 16 at $\tilde{K}_m = 5.5$. Finally, $(L/D)_{max}$ generally increases while undergoing shape change from dash to loiter configuration, accordingly to the considered planform variation (see Table 2).

3.2 Configuration comparison

The loiter, intermediate and dash configurations are now compared among each other in order to assess the potential of the concept to improve

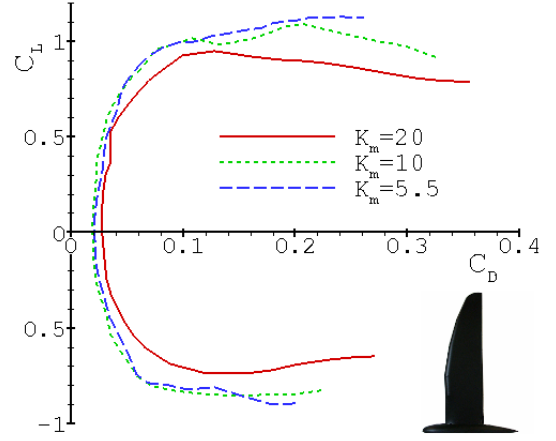


Fig. 14 Drag polars of the loiter configuration

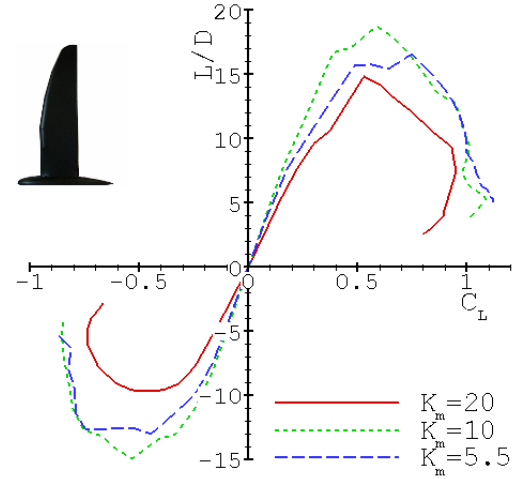


Fig. 15 Lift-to-drag ratio of the loiter configuration

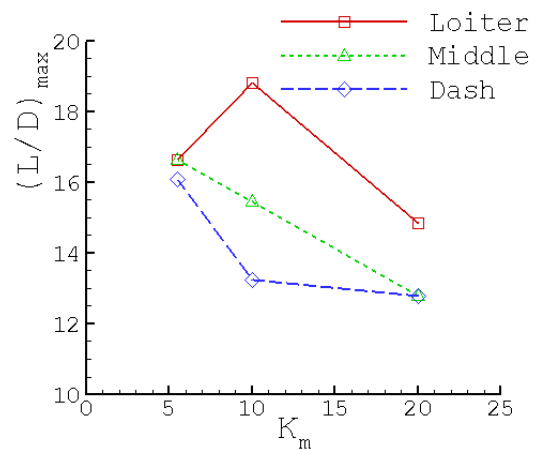


Fig. 16 Comparison of $(L/D)_{max}$ between the loiter, intermediate and dash configurations

aerodynamic efficiency over a variety of flight conditions. In order to effectively capture the benefits due to geometry change, the aerodynamic coefficients C_L and C_D multiplied by the respective reference area S_{ref} of each configuration are used here instead of the classical aerodynamic coefficients.

Fig. 17 compares the drag polars of the loiter,

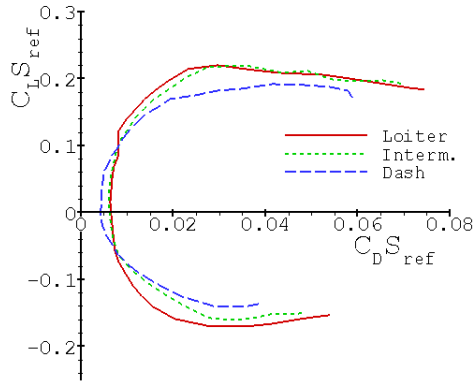
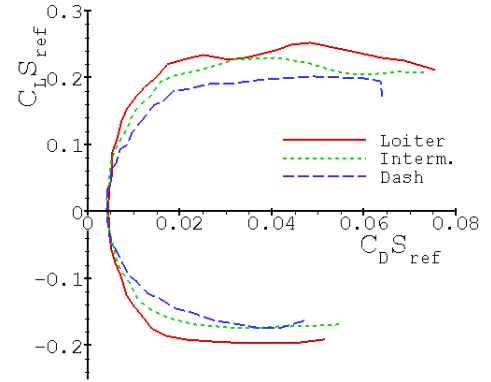


Fig. 17 Drag polars at $\tilde{K}_m = 20$

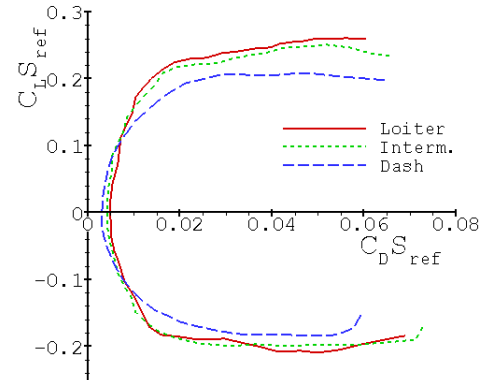
intermediate and dash configurations for the case $\tilde{K}_m = 20$ (lowest aerodynamic loading). According to the decrease in span and wetted area while undergoing shape change from loiter to dash configuration (see Fig. 5), the dash configuration exhibits the lowest drag at zero lift $C_{D0}S_{ref}$ and offers therefore advantageous drag characteristics in the lower range of $C_L S_{ref}$ compared to the other ones. In contrast, the higher aspect ratio of the loiter configuration leads to a lower induced drag, providing thus an overall lower drag in the higher range of $C_L S_{ref}$. A significant variation in aspect ratio is thus the key to obtain the widest variation in lift and drag characteristics.

The drag polars at $\tilde{K}_m = 10$ and $\tilde{K}_m = 5.5$ given in Fig. 18 exhibit qualitatively the same features. However, the tendencies are strongly attenuated by $\tilde{K}_m = 10$.

In all cases, the drag polar of the intermediate configuration is situated just between the other configurations, ensuring a smooth transition between loiter and dash. The plots of L/D versus $C_L S_{ref}$, given in Fig. 19 show that, through alteration of the shape between loiter and dash configuration, the wing effectively offers the possibility



(a) $\tilde{K}_m = 10$



(b) $\tilde{K}_m = 5.5$

Fig. 18 Drag polars at $\tilde{K}_m = 10$ and $\tilde{K}_m = 5.5$

to fly a variety of missions (i.e. required $C_L S_{ref}$) with a higher lift-to-drag ratio than a single configuration would do.

4 Conclusion and outlook

This paper considered the experimental investigation of an elasto-flexible morphing wing concept allowing massive variation of the planform as well as in-plane geometry. For this, a wind tunnel model consisting of an articulated leading edge spar over which an elasto-flexible fabric is spanned was designed and built. The actively controlled configuration of the leading edge spar thereby sets the overall planform of the wing, whereas the membrane passively deforms under aerodynamic loading. A set of three discrete configurations of the wing consisting of a high aspect ratio, straight wing (loiter configuration), a

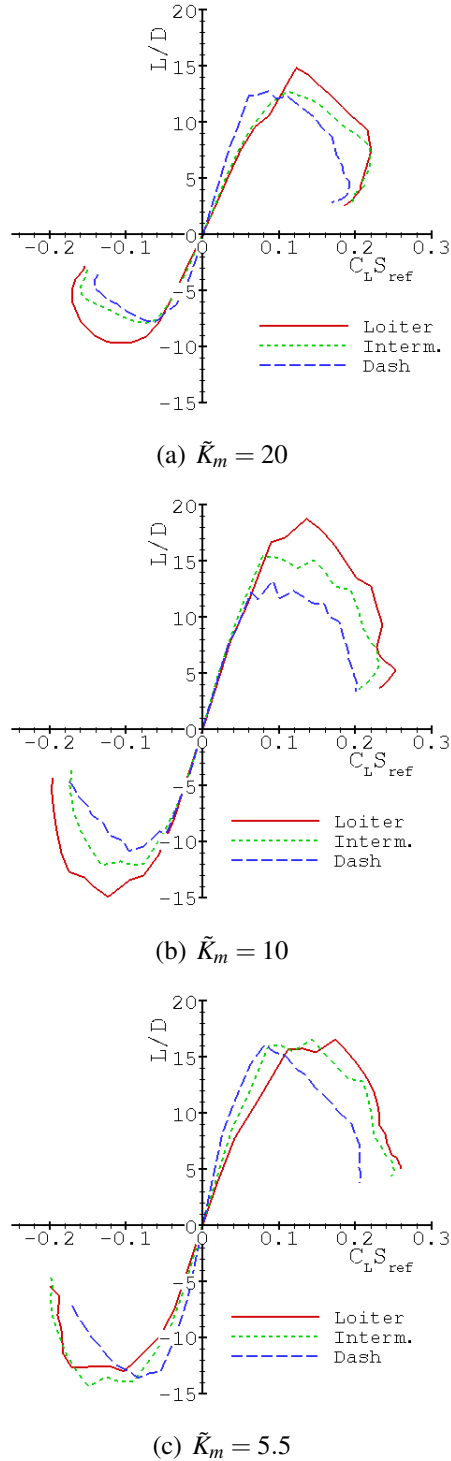


Fig. 19 Drag polars and L/D versus $C_L S_{ref}$

low aspect ratio, swept back wing (dash configuration) and an intermediate configuration were tested at three different wind speeds. Through force measurements combined with wool tuft experiment and visualization of the

wing deformation, the particular behavior of the wing resulting from the highly elastic wing construction could be assessed. It was shown that the in-plane shape of the wing (i.e. camber distribution) is very sensitive to the flow condition via the dynamic pressure and angle of attack. As a result of this so called "passive morphing", the lift and drag characteristics of the wing showed a pronounced dependency to the aerodynamic loading as well. Beside the mild stall characteristics observed, the exhibited dynamic pressure dependency of the maximum lift-to-drag ratio indicate that there may be an optimal deformation state (i.e. resulting airfoil distribution) leading to the best aerodynamic efficiency.

Future work will focus on the detailed investigation (experimental as well as numerical) of the membrane deformation to predict its aero-elastic interaction with the airflow. A long term aim thereby is to be able to design a fabric with targeted properties leading to an optimized wing behavior.

Beside this, the comparison of the configurations among each other confirmed the potential of this morphing concept to improve efficiency over a variety of flight conditions. Thereby, the importance of a significant variation in aspect ratio while undergoing shape change to obtain the largest variation in lift and drag characteristics could be demonstrated. The loiter and dash configuration respectively were shown to offer superior efficiency over distinct ranges of flight conditions (i.e. flight speed) and, effectively contributing to performances improvement.

Future work will also involve a systematic investigation of configurations out of the current achievable range in order to assess the full potential of this morphing concept.

References

- [1] John D. Anderson. *Aircraft Performances and Design*. McGraw-Hill International Editions, 1996.
- [2] M. Fluck. Der pterosaurus flügel - eine flexible, tragende fläche. Term Paper.
- [3] L. W. Kehong and J. D. Jacob. In flight aspect

ratio morphing using inflatable wings. In *45th AIAA Aerospace Sciences Meeting and Exhibit*, January 2008.

- [4] H. Murai and S. Maruyama. Theoretical investigation of the aerodynamics of double membrane sailing airfoil section. *Journal of Aircraft*, 17(5):294–299, 1980.
- [5] K. Padian and J. M. V Rayner. The wing of pterosaurs. *American Journal of Science*, 293-A:91–166, 1993.
- [6] A. R. Rodriguez. Morphing aircraft technology survey. In *45th AIAA Aerospace Sciences Meeting and Exhibit*, January 2007.
- [7] R. Smith and W. Shyy. Computation of unsteady flow over a flexible two-dimensional membrane wing. *Physics of fluids*, 7(9).
- [8] R. M. Waldman and A. J. Song. Aerodynamic behavior of compliant membranes as related to bat flight. Number AIAA-2008-3716.

Copyright Statement

The authors confirm that they, and/or their company or organization, hold copyright on all of the original material included in this paper. The authors also confirm that they have obtained permission, from the copyright holder of any third party material included in this paper, to publish it as part of their paper. The authors confirm that they give permission, or have obtained permission from the copyright holder of this paper, for the publication and distribution of this paper as part of the ICAS2010 proceedings or as individual off-prints from the proceedings.